



HAL
open science

A Proper Generalized Decomposition based solver for nonlinear magneto-thermal problems

Zhi Qin, Hakeim Talleb, Zhuoxiang Ren

► **To cite this version:**

Zhi Qin, Hakeim Talleb, Zhuoxiang Ren. A Proper Generalized Decomposition based solver for nonlinear magneto-thermal problems. IEEE Transactions on Magnetics, 2015, 52 (2), pp.7400209-10.1109/TMAG.2015.2492462 . hal-01229635

HAL Id: hal-01229635

<https://hal.sorbonne-universite.fr/hal-01229635>

Submitted on 7 Apr 2016

HAL is a multi-disciplinary open access archive for the deposit and dissemination of scientific research documents, whether they are published or not. The documents may come from teaching and research institutions in France or abroad, or from public or private research centers.

L'archive ouverte pluridisciplinaire **HAL**, est destinée au dépôt et à la diffusion de documents scientifiques de niveau recherche, publiés ou non, émanant des établissements d'enseignement et de recherche français ou étrangers, des laboratoires publics ou privés.

A Proper Generalized Decomposition-Based Solver for Nonlinear Magneto-thermal Problems

Zhi Qin, Hakeim Talleb, and Zhuoxiang Ren

Sorbonne Universités, University Pierre et Marie Curie–Université Paris 06, Paris F-75005, France

This paper investigates solving coupled magneto-thermal problems through a proper generalized decomposition-based non-incremental approach. The magnetodynamic and thermodynamic problems are strongly coupled as the electric material property changes with the temperature while the temperature field evolves due to the Joule heat generated by induced currents. A challenge to solve the coupled problem is that the electric time constant can be several orders of magnitude smaller than the thermal one. Solution through a classical time integration approach requires too many time steps, especially when a long duration needs to be simulated, hence making the problem size too large to be handled. The proposed solver overcomes this difficulty through decomposing unknown dynamic fields into the space and time modes and solving the linearized systems in space and time iteratively, using the finite element method. The material nonlinearity can be incorporated in a straightforward way. The advantages of the proposed solver are demonstrated in solving an academic problem.

Index Terms—Finite elements in space and time, magneto-thermal coupling, model reduction, proper generalized decomposition (PGD).

I. INTRODUCTION

NUMERIC simulation plays an important role in studying time-dependent physics problems. Classical strategies to conduct such simulations consist of discretizing the model in space and solving the resultant ordinary differential equations (ODEs) with time integration. It can be inapplicable in the cases where a large number of time steps is involved or a huge amount of results needs to be stored [1]. An alternative way is to project the initial model onto a reduced basis and solve a system of smaller size, which effectively alleviates computing burdens. The idea is realized thanks to the proper generalized decomposition (PGD) method [2] and developed into the so-called non-incremental space–time separation method [3].

In general, the reduced basis of the dynamic problem can be constructed either *a posteriori* or *a priori*. When constructed *a posteriori*, the initial problem needs to be solved, after which reduced basis can be obtained through the decomposition of the calculated results into the space–time modes. Techniques, such as the singular value decomposition (SVD) or the proper orthogonal decomposition [4], can be employed for such purposes. For constructions *a priori*, the pre-calculation of the unknown fields is unnecessary. Instead, the unknowns are assumed as a sum of space–time modes that can be obtained through an enrichment process. Each enrichment step consists of calculating one pair of space and time modes simultaneously. Iterations in the enrichments usually converge in a moderate number of steps, leading to a significant decline in the problem size compared with the conventional methods [2]. Moreover, the representation of unknown dynamic fields over the whole space–time domain can then be achieved with the obtained modes, whose size can be much smaller than that obtained with a classical solver. The PGD-based space–time separated method witnessed many applications,

especially on mechanics. For instance, it is employed to solve the problems of rheology [5], viscoelasticity [6], fluid flow [7], and elastodynamics [8]. A dedicated review is found in [4]. In the electromagnetic community, the applications of PGD on the magnetostatic field problems are now available [9].

Nevertheless, applying the new methodology to the cases where dynamic electromagnetic fields are involved remains to be exploited. Meanwhile, dynamic multi-physics problems with distinct time constants are very common. Taking the coupled magneto-thermal problem, for instance, both the magnetic and thermal fields depend on each other, since the material properties are temperature dependent and that time varying magnetic fields induce eddy current in the conducting area which, in turn, generates heat and affects the temperature field. The difference between the characteristic time constants of the fields can be very large, particularly for high-frequency current exciting cases. Solving the coupled problem with time integration requires the time steps to be set according to the smallest time constant that can be very small. For example, to simulate temperature rise due to a 1 kHz source current during 1 min needs at least 6×10^5 steps with a minimum of ten time steps per period, regardless of extra steps stemming from the material nonlinearity. For realistic large-size 3-D cases, the time integration approach is apparently impractical. Solving the problem in frequency domain using the harmonic balance method [10] providing an alternative though the calculating burden may not be significantly decreased.

In this paper, a non-incremental solver applying the space–time separation strategy to such magnetodynamic multi-physics problems is developed. In addition to a huge potential of reducing calculating costs, the proposed solver provides a convenient way to account for the temperature dependence of material properties. The remaining sections are

organized as follows. In Section II, the coupled problem is presented. A conventional time integration approach is recalled in Section III. The non-incremental solver is introduced in Section IV, followed by numerical examples in Section V. Section VI provides the concluding remarks and perspectives.

II. COUPLED NONLINEAR DYNAMIC PROBLEM

A. Magnetic Problem

Solving magnetodynamic problems with the finite element method has been investigated by many researchers, e.g., the authors in [11] and [12] among others. In view of that, a large portion of magnetodynamic applications is axisymmetric, formulations in cylindrical coordinates will be considered in what follows. Primary procedures and notations are adapted from [11]. Denote \vec{B} , \vec{H} , \vec{E} , and \vec{J} , respectively, as the magnetic induction, magnetic field, electric field, and electric current density. The governing equations of the eddy current problem and the material constitutive laws read as in (1) and (2), respectively

$$\nabla \times \vec{E} = -\partial \vec{B} / \partial t \quad (1a)$$

$$\nabla \times \vec{H} = \vec{J} \quad (1b)$$

$$\vec{B} = \mu \vec{H} \quad (2a)$$

$$\vec{J} = \sigma \vec{E} \quad (2b)$$

where μ and σ depict the magnetic permeability and the electric conductivity, respectively. The electric conductivity σ depends on the temperature field T in the current case, which reads

$$\sigma = \mathcal{F}(T). \quad (3)$$

Introducing the magnetic vector potential \vec{A} as in (4) yields relation (5)

$$\vec{B} = \nabla \times \vec{A} \quad (4)$$

$$\nabla \times \vec{E} = -\nabla \times \partial \vec{A} / \partial t. \quad (5)$$

It can be deduced from (5) that

$$\vec{E} = -\partial \vec{A} / \partial t - \nabla V \quad (6)$$

where V represents an unknown electric potential.

The current term \vec{J} is a sum of eddy current \vec{J}_e and source current \vec{J}_s , with \vec{J}_e expressed as in

$$\vec{J}_e = \sigma(-\partial \vec{A} / \partial t - \nabla V). \quad (7)$$

Thus, the constitutive equation for eddy current problem can be expressed as

$$\nabla \times \frac{1}{\mu} (\nabla \times \vec{A}) = \sigma(-\partial \vec{A} / \partial t - \nabla V) + \vec{J}_s \quad (8)$$

which is to be solved with gauging conditions.

In the axisymmetric case, only the φ components of \vec{A} , \vec{J}_e , and \vec{J}_s , i.e., A_φ , $J_{e\varphi}$, and $J_{s\varphi}$, are non-vanishing. In this condition, the variable V disappears and the current density is expressed by $J_{e\varphi} = -\sigma \partial A_\varphi / \partial t$. The gauging condition is satisfied when Dirichlet conditions are applied to A_φ . Equation (8) can, thus, be simplified into a scalar function

$$\sigma \frac{\partial A_\varphi}{\partial t} + \frac{\partial}{\partial r} \left(\frac{1}{\mu r} \frac{\partial (r A_\varphi)}{\partial r} \right) + \frac{\partial}{\partial z} \left(\frac{1}{\mu} \frac{\partial A_\varphi}{\partial z} \right) = J_{s\varphi}. \quad (9)$$

Introducing a new variable

$$A = r A_\varphi \quad (10)$$

gives the equation of interest

$$\frac{\sigma}{r} \dot{A} + \frac{\partial}{\partial r} \left(\frac{1}{\mu r} \frac{\partial A}{\partial r} \right) + \frac{\partial}{\partial z} \left(\frac{1}{\mu r} \frac{\partial A}{\partial z} \right) = J \quad (11)$$

where $\dot{A} = \partial A / \partial t$ and $J = J_\varphi$.

Let Ω^A denote the magnetic domain whose boundary Γ^A can be parted as a sum of Dirichlet boundaries Γ_D^A and Neumann boundaries Γ_N^A . Boundary conditions for A can be formulated as

$$\begin{aligned} A &= \hat{A} \text{ on } \Gamma_D^A \\ \partial A / \partial n &= \hat{\Psi}_A \text{ on } \Gamma_N^A \end{aligned} \quad (12)$$

where n indicates the unit vector of outward direction and normal to Γ_N .

Initial condition for A can be expressed by

$$A = A_0 \text{ at } t = 0. \quad (13)$$

B. Thermal Problem

The thermal problem is governed by the heat transfer equation

$$\rho C_p \partial T / \partial t - \nabla \cdot (\kappa \nabla T) = Q_T \quad (14)$$

where ρ is the mass density, C_p is the specific heat capacity, κ is the thermal conductivity, and the heat source Q_T that comes from Joule heating of the induced eddy currents reads [12]

$$Q_T = \sigma \left(\frac{\partial A}{r \partial t} \right)^2. \quad (15)$$

Rewriting (14) in cylindrical coordinates gives

$$\rho C_p \dot{T} - \kappa \frac{\partial^2 T}{\partial r^2} - \kappa \frac{\partial^2 T}{\partial z^2} = \sigma \left(\frac{\partial A}{r \partial t} \right)^2 \quad (16)$$

with $\dot{T} = \partial T / \partial t$.

The initial condition for T is

$$T = T_0 \text{ at } t = 0. \quad (17)$$

Boundary conditions are

$$\begin{aligned} T &= \hat{T} \text{ on } \Gamma_D^T \\ -\kappa \cdot \partial T / \partial n &= \hat{Q}_T \text{ on } \Gamma_N^T \end{aligned} \quad (18)$$

where Γ_D^T and Γ_N^T are, respectively, the Dirichlet and Neumann boundaries of the thermal problem domain Ω^T .

III. CONVENTIONAL TIME INTEGRATION APPROACH

A. Finite Element Formulations

Weak forms of the coupled problem can be obtained using the variational principle. Let us begin with multiplying

(11) by (16) with test functions A^* and T^* before integrating over domains Ω^A and Ω^T , respectively, which yields

$$\int_{\Omega} A^* \left\{ \frac{\sigma}{r} \dot{A} + \frac{\partial}{\partial r} \left(\frac{1}{\mu r} \frac{\partial A}{\partial r} \right) + \frac{\partial}{\partial z} \left(\frac{1}{\mu r} \frac{\partial A}{\partial z} \right) - J \right\} d\Omega = 0 \quad (19a)$$

$$\int_{\Omega} T^* \left\{ \rho C_p \dot{T} - \kappa \frac{\partial^2 T}{\partial r^2} - \kappa \frac{\partial^2 T}{\partial z^2} - \sigma \left(\frac{\partial A}{r \partial t} \right)^2 \right\} d\Omega = 0. \quad (19b)$$

The space domain is discretized through a triangulation \mathcal{T}_h . As the magnetic and thermal fields are coupled in a strong fashion and A and T depend on each other, both the magnetic and thermal problems can be analyzed on the same space mesh $\Omega_h = \bigcup_{i=1}^{N_s^{\text{ele}}} \Omega_e^i$ consisting of N_s^{node} nodes in N_s^{ele} elements. Meanwhile, r and σ in (19) in Ω_e^i can be replaced by \bar{r}_i and σ_i , respectively. For simplicity, the values of r and σ at the barycentric coordinate of each element are taken. As such, techniques developed for conventional Cartesian coordinate system-based problems can be adapted. The weak form is expressed as in

$$\sum_{i=1}^{N_s^{\text{ele}}} \int_{\Omega_e^i} \left\{ \frac{\sigma_i}{\bar{r}_i} A^* \dot{A} + \frac{1}{\mu \bar{r}_i} \left(\frac{\partial A^*}{\partial r} \frac{\partial A}{\partial r} + \frac{\partial A^*}{\partial z} \frac{\partial A}{\partial z} \right) - A^* J \right\} d\Omega = 0 \quad (20a)$$

$$\sum_{i=1}^{N_s^{\text{ele}}} \int_{\Omega_e^i} \left\{ \rho C_p T^* \dot{T} - \kappa \left(\frac{\partial T^*}{\partial r} \frac{\partial T}{\partial r} + \frac{\partial T^*}{\partial z} \frac{\partial T}{\partial z} \right) - \frac{\sigma_i}{\bar{r}_i^2} T^* \dot{A}^2 \right\} d\Omega = 0. \quad (20b)$$

Next, field unknowns in each element are interpolated in terms of nodal degrees of freedom (DoFs) using appropriate basis functions. As an example, values of A and T at a point \underline{X} [or at (r, φ, z)] in element Ω_e^k can be expressed as products of basis functions $\underline{N}(\underline{X})$ and nodal DoFs \underline{A}_k (respectively, \underline{T}_k)

$$A(\underline{X}) = \underline{N}(\underline{X})^T \cdot \underline{A}_k \quad (21a)$$

$$T(\underline{X}) = \underline{N}(\underline{X})^T \cdot \underline{T}_k. \quad (21b)$$

Taking into account the boundary conditions in (20) yields a system of ODEs with respect to the time t , as shown in

$$\underline{\underline{C}}_A(\underline{T}) \cdot \dot{\underline{A}} + \underline{\underline{K}}_A \cdot \underline{A} = \underline{J} \quad (22a)$$

$$\underline{\underline{C}}_T \cdot \dot{\underline{T}} + \underline{\underline{K}}_T \cdot \underline{T} = \underline{Q}(\underline{T}, \underline{A}) \quad (22b)$$

where matrices and vectors are defined as in

$$\underline{\underline{C}}_A(\underline{T}) = \sum_{i=1}^{N_s^{\text{ele}}} \int_{\Omega_e^i} \frac{\sigma_i(\underline{T})}{\bar{r}_i} \underline{N}^T \underline{N} d\Omega \quad (23a)$$

$$\underline{\underline{K}}_A = \sum_{i=1}^{N_s^{\text{ele}}} \int_{\Omega_e^i} \frac{1}{\mu \bar{r}_i} \nabla \underline{N}^T \nabla \underline{N} d\Omega \quad (23b)$$

$$\underline{J} = \sum_{i=1}^{N_s^{\text{ele}}} \int_{\Omega_e^i} \underline{N}^T \underline{N} d\Omega \underline{J}_i \quad (23c)$$

$$\underline{\underline{C}}_T = \sum_{i=1}^{N_s^{\text{ele}}} \int_{\Omega_e^i} \rho C_p \underline{N}^T \underline{N} d\Omega \quad (23d)$$

$$\underline{\underline{K}}_T = \sum_{i=1}^{N_s^{\text{ele}}} \int_{\Omega_e^i} \kappa \nabla \underline{N}^T \nabla \underline{N} d\Omega \quad (23e)$$

$$\underline{Q}(\underline{T}, \underline{A}) = \sum_{i=1}^{N_s^{\text{ele}}} \int_{\Omega_e^i} \frac{\sigma_i(\underline{T})}{\bar{r}_i^2} \left(\frac{\partial A_i}{\partial t} \right)^2 \underline{N}^T \underline{N} d\Omega \quad (23f)$$

and \underline{A} and \underline{T} are the DoFs to be computed; terms associated with Neumann boundary conditions can be added to the r.h.s. terms.

B. Time Integration and Handling Nonlinearity

The Crank–Nicholson time discretization schema is one of the most used time integration methods to solve (22) step by step. To account for material nonlinearity, the Picard iteration (also referred to as the fixed-point method) or the Newton iteration can be employed within each time step. However, the Newton method can be intractable in the present case, since it necessitates the calculating derivatives of the nonlinear terms with respect to A and T , which can be too involved and too costly [10]. Therefore, the Picard method that linearizes the system at the current step by simply substituting DoFs from the previous iteration into the nonlinear terms should be preferable. As shown in (24), at the $(k+1)$ th step, \underline{A}_k and \underline{T}_k obtained from the k th step are used as initial values for \underline{A}_{k+1}^p and \underline{T}_{k+1}^p ; $\underline{A}_{k+1}^{p+1}$ and $\underline{T}_{k+1}^{p+1}$ can then be calculated from linear system (24). Subsequent iterations repeat when p increases from 1 to the maximum iteration number $N_{\text{max}}^{\text{ite}}$

$$\underline{\underline{C}}_A(\underline{T}_{k+1}^p) \cdot \dot{\underline{A}}_{k+1}^{p+1} + \underline{\underline{K}}_A \cdot \underline{A}_{k+1}^{p+1} = \underline{J} \quad (24a)$$

$$\underline{\underline{C}}_T \cdot \dot{\underline{T}}_{k+1}^{p+1} + \underline{\underline{K}}_T \cdot \underline{T}_{k+1}^{p+1} = \underline{Q}(\underline{T}_{k+1}^p, \underline{A}_{k+1}^p). \quad (24b)$$

Iterations terminate when either $N_{\text{max}}^{\text{ite}}$ is reached or convergence condition (25) is met, where ε_{tol} is a prescribed value

$$\max \left(\frac{\|\underline{A}_{k+1}^{p+1} - \underline{A}_{k+1}^p\|}{\|\underline{A}_{k+1}^p\|}, \frac{\|\underline{T}_{k+1}^{p+1} - \underline{T}_{k+1}^p\|}{\|\underline{T}_{k+1}^p\|} \right) < \varepsilon_{\text{tol}}. \quad (25)$$

\underline{A}_{k+1} and \underline{T}_{k+1} are obtained as

$$\underline{A}_{k+1} = \underline{A}_{k+1}^{p+1} \quad (26a)$$

$$\underline{T}_{k+1} = \underline{T}_{k+1}^{p+1}. \quad (26b)$$

However, it is well known that the Picard iteration method may converge poorly or even fail to converge to the correct answer for large time steps. A remedy is to calculate (27) in a Crank–Nicholson frame, but with a smaller time step Δt during which the variations in T and A are not significant. Well-developed linear solvers can also be employed directly

$$\underline{\underline{C}}_A(\underline{T}_k) \cdot \dot{\underline{A}}_{k+1} + \underline{\underline{K}}_A \cdot \underline{A}_{k+1} = \underline{J} \quad (27a)$$

$$\underline{\underline{C}}_T \cdot \dot{\underline{T}}_{k+1} + \underline{\underline{K}}_T \cdot \underline{T}_{k+1} = \underline{Q}(\underline{T}_k, \underline{A}_k). \quad (27b)$$

IV. SPACE-TIME SEPARATION APPROACH

A. Weak Formulation

In the PGD-based space-time separating approach, it is assumed that the fields A and T can be approximated as a sum of N space-time modes, as shown in (28). The objective is to calculate such modes *a priori*

$$A \approx \sum_{i=1}^N A_x^i A_t^i \quad (28a)$$

$$T \approx \sum_{i=1}^N T_x^i T_t^i. \quad (28b)$$

The source term J in (19a), on the other hand, can be determined *a posteriori* as it is already defined in the whole space-time domain

$$J = \sum_{j=1}^{n_J} J_x^j J_t^j \quad (29)$$

where n_J stands for the number of stranded inductors. It can be noticed that J_x^j stands for the unit current density in the conductor and J_t^j represents the current function.

Fields A and T are obtained in an accumulating fashion, i.e., a new mode $A_x^l A_t^l$ (respectively, $T_x^l T_t^l$) is calculated and added to the previous modes $\sum_{i=1}^{l-1} A_x^i A_t^i$ (respectively, $\sum_{i=1}^{l-1} T_x^i T_t^i$) for $l = 1, \dots, N$. This procedure is called the enrichment [3]. Assume that at the $(m+1)$ th enrichment, the first m modes of A and T are obtained. Then, A and T at the $(m+1)$ th enrichment (i.e., A_{m+1} and T_{m+1}) can be expressed as

$$A_{m+1} = \sum_{i=1}^m A_x^i A_t^i + R_A S_A \quad (30a)$$

$$T_{m+1} = \sum_{i=1}^m T_x^i T_t^i + R_T S_T \quad (30b)$$

where $R_A S_A$ and $R_T S_T$ are the searched new modes with R_A and R_T related to the space variables, and S_A and S_T to the time variables, for, respectively, the magnetic and thermal problems. After normalization, $A_x^{m+1} A_t^{m+1}$ and $T_x^{m+1} T_t^{m+1}$ can be calculated from $R_A S_A$ and $R_T S_T$, respectively. Weak form can be obtained in a similar fashion as in the previous approach except that the integral domain is the whole space-time domain $\Omega \otimes I$, with Ω denoting the spatial domain while I denoting the time duration.

To linearize the nonlinear terms σ and \dot{A}^2 during the calculation of new modes, the Picard method is applied. In particular, instead of expressing σ as a function of $\sum_{i=1}^m T_x^i T_t^i + R_T S_T$ at the $(m+1)$ th enrichment, it is calculated from the first m modes of T , and denoted as σ_m (31a). \dot{A}^2 is handled in the same fashion (31b)

$$\sigma_m = \mathcal{F} \left(\sum_{i=1}^m T_x^i T_t^i \right) \quad (31a)$$

$$\dot{A}^2 = \left(\sum_{i=1}^m A_x^i \frac{A_t^i}{\partial t} \right)^2. \quad (31b)$$

Hence, the weak form can be given as in

$$\iint_{\Omega \otimes I} A^* \left\{ \begin{array}{l} \frac{\sigma_m}{r} \frac{\partial (\sum_{i=1}^m A_x^i A_t^i + R_A S_A)}{\partial t} \\ + \frac{\partial}{\partial r} \left(\frac{1}{\mu r} \frac{\partial (\sum_{i=1}^m A_x^i A_t^i + R_A S_A)}{\partial r} \right) \\ + \frac{\partial}{\partial z} \left(\frac{1}{\mu r} \frac{\partial (\sum_{i=1}^m A_x^i A_t^i + R_A S_A)}{\partial z} \right) \\ - \sum_{j=1}^{n_J} J_x^j J_t^j \end{array} \right\} d\Omega dI = 0 \quad (32a)$$

$$\iint_{\Omega \otimes I} T^* \left\{ \begin{array}{l} \rho C_p \frac{\partial (\sum_{i=1}^m T_x^i T_t^i + R_T S_T)}{\partial t} \\ - \kappa \frac{\partial^2 (\sum_{i=1}^m T_x^i T_t^i + R_T S_T)}{\partial r^2} \\ - \kappa \frac{\partial^2 (\sum_{i=1}^m T_x^i T_t^i + R_T S_T)}{\partial z^2} \\ - \sigma_m \left(\frac{\partial (\sum_{i=1}^m A_x^i A_t^i)}{r \partial t} \right)^2 \end{array} \right\} d\Omega dI = 0 \quad (32b)$$

where the test functions are

$$\begin{aligned} A^* &= R_A^* S_A + R_A S_A^* \\ T^* &= R_T^* S_T + R_T S_T^*. \end{aligned} \quad (33)$$

Though σ and $(\partial A / \partial t)^2$ are linearized, the resultant system is still nonlinear because both R_A (respectively, R_T) and S_A (respectively, S_T) are unknown in (32a) [respectively, (32b)]. The alternating direction method [3] comes to stage. It consists of alternatively calculating one of the two unknowns by assuming that the other is known. It is also called the fixed-point iterations [3].

B. Discretization in Space and Time

Discretize the time duration $I \equiv [0, \tau]$ with line elements I_h [see (34)] with $I_h^i = [t_{i-1}, t_i]$ and $0 = t_0 < \dots < t_{N_t^{\text{ele}}} = \tau$. Then, the discretized space-time domain can be represented as in (35), in which $\Omega_\alpha \otimes I_\beta$ depicts a space-time element

$$I_h = \bigcup_{i=1}^{N_t^{\text{ele}}} I_h^i \quad (34)$$

$$\Omega_h \otimes I_h = \sum_{\alpha=1}^{N_s^{\text{ele}}} \sum_{\beta=1}^{N_t^{\text{ele}}} \Omega_\alpha \otimes I_\beta. \quad (35)$$

The following basis functions in space and time are used to discretize the space- and time-related variables:

$$N_i \quad (i = 1, \dots, N_s^{\text{node}}), \quad L_j \quad (j = 1, \dots, N_t^{\text{node}}) \quad (36)$$

where N_s^{node} is the number of space nodes and N_t^{node} is the number of time points.

For example, the values of A and T of the k th mode ($k = 1, \dots, m$) at a point (\underline{X}, t) can be interpolated from their space and time DoFs (respectively, \underline{A}_x^k and \underline{A}_t^k) as

$$A^k(\underline{X}, t) = \left(\sum_{i=1}^{N_s^{\text{node}}} N_i(\underline{X}) A_x^{k_i} \right) \otimes \left(\sum_{j=1}^{N_t^{\text{node}}} L_j(t) A_t^{k_j} \right) \quad (37a)$$

$$T^k(\underline{X}, t) = \left(\sum_{i=1}^{N_s^{\text{node}}} N_i(\underline{X}) T_x^{k_i} \right) \otimes \left(\sum_{j=1}^{N_t^{\text{node}}} L_j(t) T_t^{k_j} \right). \quad (37b)$$

The values of A and T calculated from the k th enrichment over all space–time nodes can be expressed by second-order tensors $\underline{A}_x^k \otimes \underline{A}_t^k$ and $\underline{T}_x^k \otimes \underline{T}_t^k$, respectively. They are both of size $\mathbb{R}^{N_s^{\text{node}} * N_t^{\text{node}}}$.

The electric conductivity σ_m can be evaluated as in (38), where $\underline{\underline{\Sigma}}^m$ is a second rank tensor of size $\mathbb{R}^{N_s^{\text{node}} * N_t^{\text{node}}}$ and $(\underline{\underline{\Sigma}}^m)_{lh}$ is the scalar component at the l th row and h th column of $\sum_{i=1}^m \underline{T}_x^i \otimes \underline{T}_t^i$ with $1 \leq l \leq N_s^{\text{node}}$ and $1 \leq h \leq N_t^{\text{node}}$. In an element $\Omega_\alpha \otimes I_\beta$, σ_m can be taken as a constant value $\sigma_m^{\alpha\beta}$ (e.g., value at the barycentric coordinate). The approximating is accurate if the geometric dimensions of the element $\Omega_\alpha \otimes I_\beta$ are small enough

$$(\underline{\underline{\Sigma}}^m)_{lh} = F((\underline{\underline{T}}^m)_{lh}). \quad (38)$$

The source term $\sum_{i=1}^m \sigma_m (A_x^i (\partial A_t^i / r \partial t))^2$ from the thermal problem can be calculated following the same principle. It results in a second rank tensor $\underline{\underline{Q}}^m$ of size $\mathbb{R}^{N_s^{\text{node}} * N_t^{\text{node}}}$. Applying SVD separates it into a sum of n_Q space–time modes, as in

$$\text{SVD}(\underline{\underline{Q}}^m) = \sum_{j=1}^{n_Q} \underline{Q}_{x_j}^m \otimes \underline{Q}_{t_j}^m. \quad (39)$$

Without losing generality, let us start with calculating the space modes R_A and R_T . S_A and S_T are assigned with arbitrary values in the first iteration before taking values from previous iterations for the rest. Test functions can be expressed as

$$A^* = R_A^* S_A \quad (40a)$$

$$T^* = R_T^* S_T. \quad (40b)$$

Substituting (40) into (35) leads to (41). Note that due to the time discretization consistency [3], time basis functions in front of the time derivative term $\partial \underline{L}^T / \partial t$ is changed from \underline{L} to $\tilde{\underline{L}}$, with $\tilde{\underline{L}}$ equal to $\underline{L} + (\Delta t_\beta \cdot d\underline{L})/2$. When Neumann boundary conditions are involved, corresponding terms may be added into the stiffness matrix and r.h.s. vectors

$$\iint_{\Omega \otimes I} \left\{ \begin{aligned} & \frac{\sigma_m}{r} R_A^* R_A S_A \frac{\partial S_A}{\partial t} \\ & + \frac{R_A^*}{\mu} \left(\frac{\partial}{\partial r} \left(\frac{1}{r} \frac{\partial R_A}{\partial r} \right) + \frac{\partial}{\partial z} \left(\frac{1}{r} \frac{\partial R_A}{\partial z} \right) \right) S_A^2 \\ & + \sum_{i=1}^m \left[\begin{aligned} & \frac{\sigma_m}{r} R_A^* A_x^i S_A \frac{\partial A_t^i}{\partial t} \\ & + \frac{R_A^*}{\mu} \frac{\partial}{\partial r} \left(\frac{1}{r} \frac{\partial A_x^i}{\partial r} \right) S_A A_t^i \\ & + \frac{R_A^*}{\mu} \frac{\partial}{\partial z} \left(\frac{1}{r} \frac{\partial A_x^i}{\partial z} \right) S_A A_t^i \end{aligned} \right] \\ & - \sum_{j=1}^{n_J} R_A^* J_x^j S_A J_t^j \end{aligned} \right\} d\Omega dI = 0 \quad (41a)$$

$$\iint_{\Omega \otimes I} \left\{ \begin{aligned} & \rho C_p R_T^* R_T S_T \frac{\partial S_T}{\partial t} \\ & - \kappa R_T^* \left(\frac{\partial^2 R_T}{\partial r^2} + \frac{\partial^2 R_T}{\partial z^2} \right) S_T^2 \\ & + \sum_{i=1}^m \left[\begin{aligned} & \rho C_p R_T^* T_x^i S_T \frac{\partial T_t^i}{\partial t} \\ & - \kappa R_T^* \left(\frac{\partial^2 T_x^i}{\partial r^2} + \frac{\partial^2 T_x^i}{\partial z^2} \right) S_T T_t^i \end{aligned} \right] \\ & - \sum_{j=1}^{n_J} R_A^* Q_x^j S_A Q_t^j \end{aligned} \right\} d\Omega dI = 0. \quad (41b)$$

Discretizing (41) yields two sets of linear equations as follows:

$$\iint_{\Omega \otimes I} \left\{ \begin{aligned} & \frac{\sigma_m^{\alpha\beta}}{r_\alpha} \underline{N} \underline{N}^T \underline{R}_{A_\alpha} \otimes \underline{S}_{A_\beta}^T \tilde{\underline{L}} \partial \underline{L}^T / \partial t \underline{S}_{A_\beta} \\ & + \frac{1}{r_{\alpha\mu}} \nabla \underline{N} \nabla \underline{N}^T \underline{R}_{A_\alpha} \otimes \underline{S}_{A_\beta}^T \underline{L} \underline{L}^T \underline{S}_{A_\beta} \\ & + \sum_{i=1}^m \left[\begin{aligned} & \frac{\sigma_m^{\alpha\beta}}{r_\alpha} \underline{N} \underline{N}^T \underline{A}_{x_\alpha}^i \otimes \underline{S}_{A_\beta}^T \tilde{\underline{L}} \partial \underline{L}^T / \partial t \underline{A}_{t_\beta}^i \\ & + \frac{1}{r_{\alpha\mu}} \nabla \underline{N} \nabla \underline{N}^T \underline{A}_{x_\alpha}^i \otimes \underline{S}_{A_\beta}^T \underline{L} \underline{L}^T \underline{A}_{t_\beta}^i \end{aligned} \right] \\ & - \sum_{j=1}^{n_J} \underline{N} \underline{N}^T \underline{J}_{x_\alpha}^j \otimes \underline{S}_{A_\beta}^T \underline{L} \underline{L}^T \underline{J}_{t_\beta}^j \end{aligned} \right\} d\Omega dI = 0 \quad (42a)$$

$$\iint_{\Omega \otimes I} \left\{ \begin{aligned} & \rho C_p \underline{N} \underline{N}^T \underline{R}_{T_\alpha} \otimes \underline{S}_{T_\beta}^T \tilde{\underline{L}} \partial \underline{L}^T / \partial t \underline{S}_{T_\beta} \\ & - \kappa \nabla \underline{N} \nabla \underline{N}^T \underline{R}_{T_\alpha} \otimes \underline{S}_{T_\beta}^T \underline{L} \underline{L}^T \underline{S}_{T_\beta} \\ & + \sum_{i=1}^m \left[\begin{aligned} & \rho C_p \underline{N} \underline{N}^T \underline{T}_{x_\alpha}^i \otimes \underline{S}_{T_\beta}^T \tilde{\underline{L}} \partial \underline{L}^T / \partial t \underline{T}_{t_\beta}^i \\ & - \kappa \nabla \underline{N} \nabla \underline{N}^T \underline{T}_{x_\alpha}^i \otimes \underline{S}_{T_\beta}^T \underline{L} \underline{L}^T \underline{T}_{t_\beta}^i \end{aligned} \right] \\ & - \sum_{j=1}^{n_J} \underline{N} \underline{N}^T \underline{Q}_{x_{j\alpha}}^m \otimes \underline{S}_{A_\beta}^T \underline{L} \underline{L}^T \underline{Q}_{t_{j\beta}}^m \end{aligned} \right\} d\Omega dI = 0 \quad (42b)$$

where \underline{N} is the space basis function associated with the space nodes in Ω_α and \underline{L} is the time basis functions associated with the time nodes in I_β .

Integrating over space and time followed by assembling the elemental matrices into global level yields linear equations for \underline{R}_A and \underline{R}_T

$$\begin{aligned} & [\hat{\underline{C}}_{\underline{A}} + (\underline{S}_{\underline{A}}^T \underline{M}_{\underline{A}} \underline{S}_{\underline{A}}) \underline{K}_{\underline{A}}] \underline{R}_A \\ & = - \sum_{i=1}^m [\check{\underline{C}}_{\underline{A}} + (\underline{S}_{\underline{A}}^T \underline{M}_{\underline{A}} \underline{A}_t^i) \underline{K}_{\underline{A}}] \underline{A}_x^i + \sum_{j=1}^{n_J} (\underline{S}_{\underline{A}}^T \underline{M}_{\underline{A}} \underline{J}_t^j) \underline{M}_{\underline{A}} \underline{J}_x^j \end{aligned} \quad (43a)$$

$$\begin{aligned} & [(\underline{S}_{\underline{T}}^T \underline{K}_{\underline{T}} \underline{S}_{\underline{T}}) \underline{C}_{\underline{T}} + (\underline{S}_{\underline{T}}^T \underline{M}_{\underline{T}} \underline{S}_{\underline{T}}) \underline{K}_{\underline{T}}] \underline{R}_T \\ & = - \sum_{i=1}^m [(\underline{S}_{\underline{T}}^T \underline{K}_{\underline{T}} \underline{T}_t^i) \underline{C}_{\underline{T}} + (\underline{S}_{\underline{T}}^T \underline{M}_{\underline{T}} \underline{T}_t^i) \underline{K}_{\underline{T}}] \underline{T}_x^i \\ & + \sum_{j=1}^{n_J} (\underline{S}_{\underline{T}}^T \underline{M}_{\underline{T}} \underline{Q}_{t_j}^m) \underline{M}_{\underline{T}} \underline{Q}_{x_j}^m. \end{aligned} \quad (43b)$$

Coefficient matrices are obtained as follows:

$$\underline{K}_{\underline{A}} = \sum_{\beta=1}^{N_t^{\text{ele}}} \int_{I_\beta} \tilde{\underline{L}} \frac{\partial \underline{L}^T}{\partial t} dt \quad (44a)$$

$$\underline{M}_{\underline{A}} = \sum_{\beta=1}^{N_t^{\text{ele}}} \int_{I_\beta} \underline{L} \underline{L}^T dt \quad (44b)$$

$$\hat{\underline{C}}_{\underline{A}} = \sum_{\alpha=1}^{N_s^{\text{ele}}} \left[\left(\sum_{\beta=1}^{N_t^{\text{ele}}} \frac{\sigma_m^{\alpha\beta}}{r_\alpha} \underline{S}_{A_\beta}^T \cdot \int_{I_\beta} \tilde{\underline{L}} \partial \underline{L}^T / \partial t dt \cdot \underline{S}_{A_\beta} \right) \cdot \int_{\Omega_\alpha} \underline{N} \underline{N}^T d\Omega \right] \quad (44c)$$

$$\check{\underline{C}}_{\underline{A}} = \sum_{\alpha=1}^{N_s^{\text{ele}}} \left[\left(\sum_{\beta=1}^{N_t^{\text{ele}}} \frac{\sigma_m^{\alpha\beta}}{r_\alpha} \underline{S}_{A_\beta}^T \cdot \int_{I_\beta} \tilde{\underline{L}} \partial \underline{L}^T / \partial t dt \cdot \underline{A}_t^{i\beta} \right) \cdot \int_{\Omega_\alpha} \underline{N} \underline{N}^T d\Omega \right] \quad (44d)$$

$$\underline{K}_{\underline{A}} = \sum_{\alpha=1}^{N_s^{\text{ele}}} \int_{\Omega_\alpha} \frac{1}{r_{\alpha\mu}} \nabla \underline{N} \nabla \underline{N}^T d\Omega \quad (44e)$$

$$\underline{\underline{M}}_A = \underline{\underline{M}}_T = \sum_{\alpha=1}^{N_s^{\text{ele}}} \int_{\Omega_\alpha} \underline{N} \underline{N}^T d\Omega \quad (44f)$$

$$\underline{\underline{C}}_T = \sum_{\alpha=1}^{N_s^{\text{ele}}} \int_{\Omega_\alpha} \rho C_p \underline{N} \underline{N}^T d\Omega \quad (44g)$$

$$\underline{\underline{K}}_T = \sum_{\alpha=1}^{N_s^{\text{ele}}} \int_{\Omega_\alpha} \kappa \nabla \underline{N} \nabla \underline{N}^T d\Omega. \quad (44h)$$

C. Enrichment Procedure

Define $[\underline{A}_x]_m = [\underline{A}_x^1, \underline{A}_x^2, \dots, \underline{A}_x^m]$, likewise for $[\underline{A}_t]_m$, $[\underline{T}_x]_m$, and $[\underline{T}_t]_m$. Then, define a new tensor $\{\text{modes}\}^m$ as

$$\{\text{modes}\}^m = \bigcup ([\underline{A}_x]_m, [\underline{A}_t]_m, [\underline{T}_x]_m, [\underline{T}_t]_m). \quad (45)$$

Equation (43) can be rewritten in a more compact form as

$$\underline{R}_A = \mathcal{F}_A^s(\underline{S}_A, \{\text{modes}\}^m) \quad (46a)$$

$$\underline{R}_T = \mathcal{F}_T^s(\underline{S}_T, \{\text{modes}\}^m). \quad (46b)$$

Once calculated, \underline{R}_A and \underline{R}_T are normalized as

$$\underline{R}_A = \frac{\underline{R}_A}{\|\underline{R}_A\|}, \quad \underline{R}_T = \frac{\underline{R}_T}{\|\underline{R}_T\|}. \quad (47)$$

In the same way, functions for calculating \underline{S}_A and \underline{S}_T can be obtained as in

$$\underline{S}_A = \mathcal{F}_A^i(\underline{R}_A, \{\text{modes}\}^m) \quad (48a)$$

$$\underline{S}_T = \mathcal{F}_T^i(\underline{R}_T, \{\text{modes}\}^m). \quad (48b)$$

The normalization of \underline{R}_A and \underline{R}_T prevents cases in fixed-point iterations, where one of the space and time modes tends to be infinitely small while the other tends to be infinitely large and, thus, leads to difficulties for converging [4]. $\{\underline{R}_A, \underline{R}_T\}$ and $\{\underline{S}_A, \underline{S}_T\}$ are repeatedly updated until convergence or a maximum iteration number $N_{\text{max}}^{\text{ite}}$ is reached. As the magnetic and thermal problems may converge at different rates, it would be wise to perform iterations separately. Moreover, as suggested in Fig. 1, the two problems can be resolved in parallel, permitting a further reduction in computation time. The parallel calculation is not implemented in this paper but can be regarded as a perspective for future efficiency improvement. Convergence criterion $\varepsilon_{\text{FixIte}}$ for both the problems can be taken identically. Then, the convergence of iterations reads

$$\frac{\|\underline{S}_A^l - \underline{S}_A^{l-1}\|}{\|\underline{S}_A^{l-1}\|} \leq \varepsilon_{\text{FixIte}} \quad (49a)$$

$$\frac{\|\underline{S}_T^l - \underline{S}_T^{l-1}\|}{\|\underline{S}_T^{l-1}\|} \leq \varepsilon_{\text{FixIte}} \quad (49b)$$

where the superscript l indicates that the mode is calculated from the l th fixed-point iteration. Results are then assigned to the $(m+1)$ th modes

$$\underline{A}_x^{m+1} = \underline{R}_A, \quad \underline{A}_t^{m+1} = \underline{S}_A \quad (50a)$$

$$\underline{T}_x^{m+1} = \underline{R}_T, \quad \underline{T}_t^{m+1} = \underline{S}_T. \quad (50b)$$

The enrichment procedure terminates when the following convergence conditions is reached. A maximum enrichment

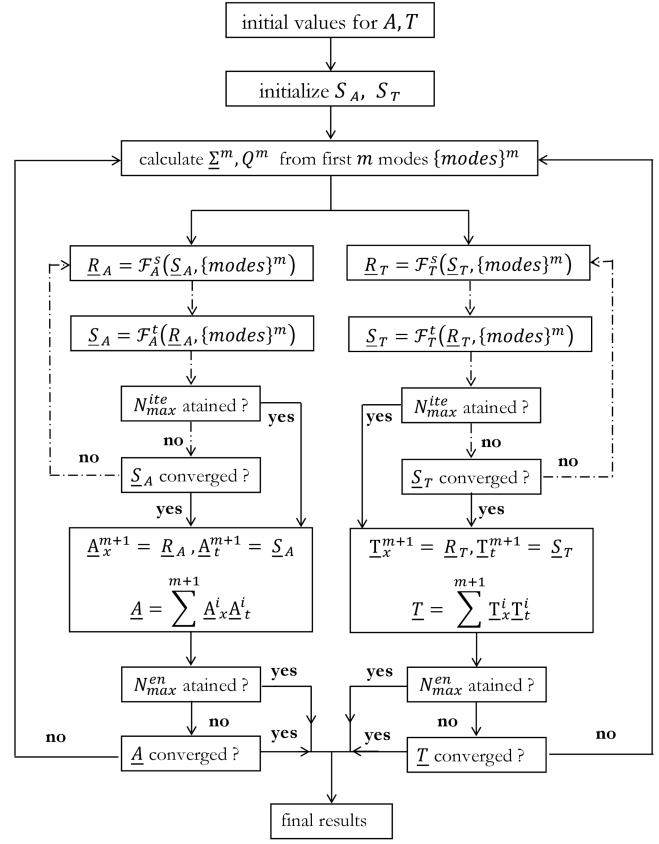


Fig. 1. Algorithm of the space-time separation solver.

number $N_{\text{max}}^{\text{en}}$ can be specified too in order to control loops numbers

$$\frac{\|\underline{A}_x^{m+1} \otimes \underline{A}_t^{m+1}\|}{\|\sum_{i=1}^{m+1} \underline{A}_x^i \otimes \underline{A}_t^i\|} \leq \varepsilon_{\text{En}} \quad (51a)$$

$$\frac{\|\underline{T}_x^{m+1} \otimes \underline{T}_t^{m+1}\|}{\|\sum_{i=1}^{m+1} \underline{T}_x^i \otimes \underline{T}_t^i\|} \leq \varepsilon_{\text{En}}. \quad (51b)$$

Other issues, such as the enforcement of non-homogeneous Dirichlet boundary conditions, can be found in [13].

Provided that overheads, such as the matrices assembling, are negligible, the computational complexity of the proposed solver can be evaluated as

$$\mathcal{C}_{\text{PGD}} = \left(\sum_{i=1}^{N_A^{\text{en}}} N_{A_i}^{\text{ite}} + \sum_{j=1}^{N_T^{\text{en}}} N_{T_j}^{\text{ite}} \right) \mathcal{C}_0 \quad (52)$$

where $\mathcal{C}_0 = \mathcal{C}(N_s^{\text{node}}) + \mathcal{C}(N_t^{\text{node}})$ is the complexity of solving an N_s^{node} -dimensional space problem and an N_t^{node} -dimensional time problem and N_X^{en} the total enrichment steps with $N_{X_i}^{\text{ite}}$ fixed-point iteration passed at its i th enrichment ($X = A, T$). The complexity of the incremental solver can be assessed as in

$$\mathcal{C}_{\text{inc}} = 2 \times N_t^{\text{node}} \cdot \mathcal{C}(N_s^{\text{node}}). \quad (53)$$

Benefits with the PGD-based solver arise when N_t^{node} is greater than $(\sum_{i=1}^{N_A^{\text{en}}} N_{A_i}^{\text{ite}} + \sum_{j=1}^{N_T^{\text{en}}} N_{T_j}^{\text{ite}})$.

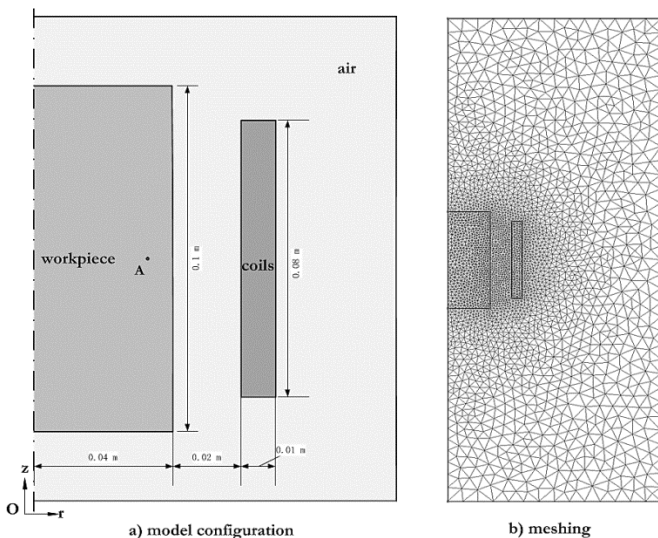


Fig. 2. Model configuration and space triangulation.

TABLE I
MAGNETIC AND THERMAL MATERIAL CONSTANTS

	Work-piece	Coil	Air
$\sigma_0 (\Omega^{-1}/m)$	$5.7013 \cdot 10^7$	0	0
$\mu_r (1)$	1	1	1
$\rho c (J/kg/K)$	$3.3495 \cdot 10^6$	$1.2 \cdot 10^3$	$1.2 \cdot 10^3$
$\kappa (W/m/k)$	400	0.02	0.02

V. NUMERICAL ILLUSTRATIONS

A. Model Configuration and Results

The proposed solver is implemented in MATLAB, which is employed to solve a coupled magnetothermal problem in which a conductor axisymmetric to the z -axis is surrounded by an excitation coil; an area of $0.2 \text{ m} \times 0.5 \text{ m}$, including the air, is considered as the solution domain. The geometric dimensions of the parts are depicted in Fig. 2. Material property constants are summarized in Table I. Temperature dependence of the electric conductivity of the workpiece is given in

$$\sigma(T) = \sigma_0 / [1 + \alpha(T - T_0)] \quad (54)$$

where α equals to $3.9 \cdot 10^{-3}$ and T_0 is set to 293.15 K.

Eddy current in the excitation coil is not accounted for in the simulation. A uniform sinusoidal electric current of 2000 kA and 100 Hz is applied to the coil. Linear triangular elements are used to discretize the space domain. The size of the elements near the conductor skin is set to be relatively smaller to account for the skin effects, and 5659 elements with 2900 nodes are generated. The total time duration is set to 0.1 s, i.e., ten periods for the electromagnetic problem.

The simulation is first carried out on a model with an extremely fine space-time mesh using the traditional incremental approach, whose outputs $\{\underline{A}\}_{\text{REF}}$ and $\{\underline{T}\}_{\text{REF}}$ are used as reference. Next, a relatively larger time increment is set while Picard nonlinear iterations are performed between two adjunct time steps. Both the simulations are carried out with a mature in-house finite element package. It is found that

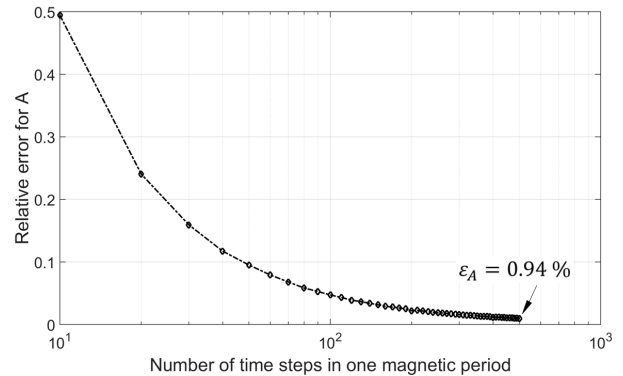


Fig. 3. Relation between relative errors and step sizes of the increment solver.

the calculation expense increases significantly in order to get a close solution to the reference one, which is less optimal. Then we resort to incremental solvers without nonlinear solvers, for which time steps need to be set as small as possible so as to limit the nonlinear effects between adjunct time steps. Denote the results obtained with the direct incremental solver as $\{\underline{A}\}_{\text{INC}}$, $\{\underline{T}\}_{\text{INC}}$. Define ϵ_r the relative error from the incremental solver as in the following equation with $X = A, T$:

$$\epsilon_r = \frac{\|\{\underline{X}\}_{\text{REF}} - \{\underline{X}\}_{\text{INC}}\|}{\|\{\underline{X}\}_{\text{REF}}\|}. \quad (55)$$

The relation of the relative errors for A as a function of time step size is illustrated in Fig. 3. Relative errors of the temperature field show a similar trend. It can be seen that the relative error goes below 1% only if over 500 steps are contained during one magnetic period, i.e., time step size decreases below $2 \cdot 10^{-5}$ s. Δt is thus fixed to $2 \cdot 10^{-5}$ s. A simulation under the same conditions is conducted with the PGD solver, whose results are noted as $\{\underline{A}\}_{\text{PGD}}$, $\{\underline{T}\}_{\text{PGD}}$. To compare the latter with the results obtained with the conventional solver, the following relative error is defined:

$$E_r = \frac{\|\{\underline{X}\}_{\text{INC}} - \{\underline{X}\}_{\text{PGD}}\|}{\|\{\underline{X}\}_{\text{INC}}\|} \quad (56)$$

where $X = A, T$.

It is found that relative errors for \underline{A} and \underline{T} between the conventional and the PGD-based solvers are 0.36% and 0.20%, respectively. As depicted in Fig. 4, good agreements are obtained between the three sets of results. Snapshots of induced current density in the conductor during the first and the ninth magnetic period obtained from both the PGD solver and the reference simulation are shown in Fig. 5. Differences between the two sets of results are barely visible. Relative errors between the two are below 1%. Impacts of the nonlinearity of σ can be observed. For example, the maximum current induced during the first period is apparently larger than that in the ninth period, which implies that the electric conductivity has diminished due to the temperature rise.

B. Convergence and Complexity

Relative errors for fixed-point iterations and enrichments can be calculated using (49) and (51), respectively. In Fig. 6

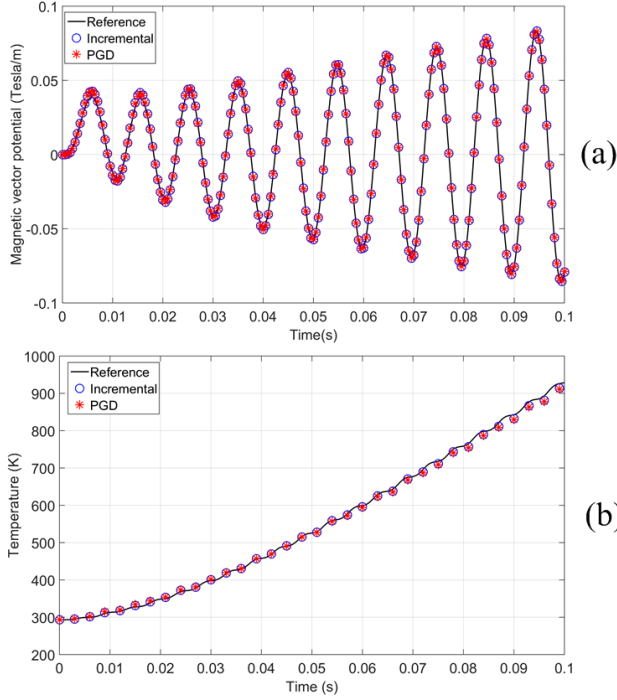


Fig. 4. Results from different solvers (a) for the magnetic problem, and (b) for the thermal problem.

are shown three kinds of typical convergence rates of the fixed-point iteration. For iterations contained in the very first enrichments, there is divergence if the maximum number of iterations is not large enough. However, it improves when more space–time modes are enriched though not reaching criterion (49a). From about the tenth enrichment on, convergence rates are accelerated in that the relative error goes below 10^{-4} after around five iterations. Maximum fixed iteration N_{\max}^{ite} is set to 10 with a stopping criterion $\varepsilon_{\text{FixIte}}$ being 10^{-4} . It is observed that most sets of fixed-point iterations converge within ten steps.

Convergence of the enrichment can be evaluated from (51) that assesses whether the norm of newly calculated space–time modes is negligible in front of the sum of all proceedings. Fig. 7 depicts the convergence history of the first 50 enrichments with and without updating. Enrichment without updating is what has been introduced in Section IV. Its convergence is not monotonous while it can still provide accurate results with a bit more space–time modes. The enrichment with updating, in contrast, gives a monotonous convergence. Updating means that after a new pair of space–time modes is added, the solver should reorder all the calculated modes in a descending sense according to their norms and then recalculate all the space and time modes with the reordered ones as initial values [4]. However, the improvements of the convergence may come at the price of a significantly increased calculating cost. It is found here that simulation time is largely extended when updating to enrichment is considered. Stopping criterion for the enrichment ε_{En} is fixed at 10^{-4} while maximum enrichment number is set to 100. Enrichments for A is stopped at its 73rd enrichment, while enrichment for T at the 81st. Total fixed-point iteration numbers for A and T are 478 and 527, respectively.

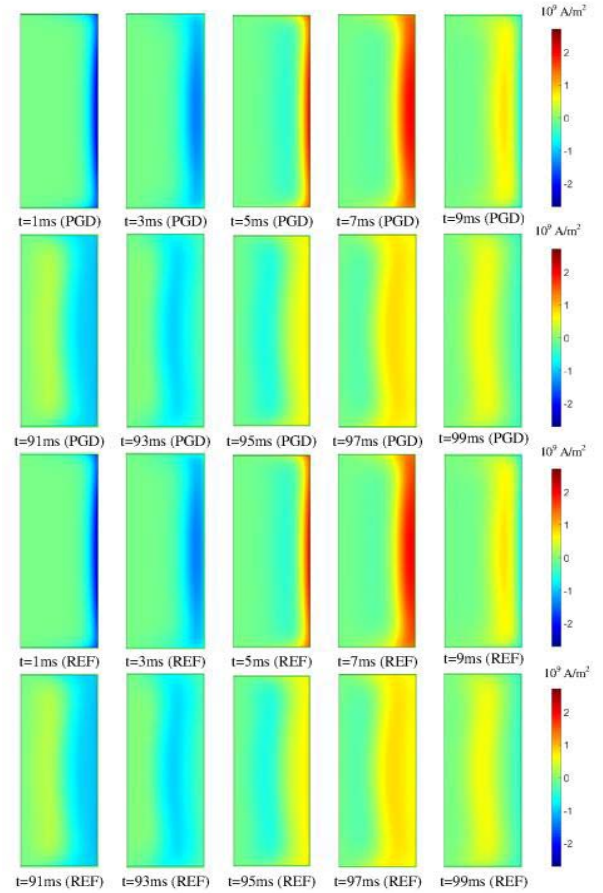


Fig. 5. Induced current density (in A/m^2) during the first (1–9 ms) and the ninth period (91–99 ms).

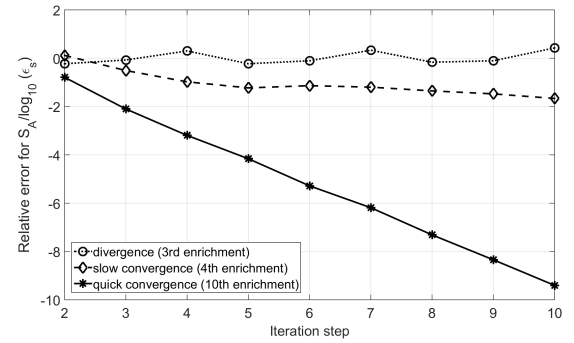


Fig. 6. Convergence rates in fixed-point iterations.

To sum up, solving the coupled magnetothermal problem with the conventional and the PGD-based solver under the same space and time discretization provides results of a difference of $<0.36\%$. In this particular case, the number of space and time nodes is respectively 2900 and 5000. Based on (52) and (53), the complexity of the conventional solver is around four times of that of the PGD-based solver. In another words, as much as 75%, costs can be saved with the non-incremental solver while no compromise on accuracy is needed. As the proposed and the conventional simulations are carried out on different platforms, a comparison of computing time does not make much sense and is not reported here.

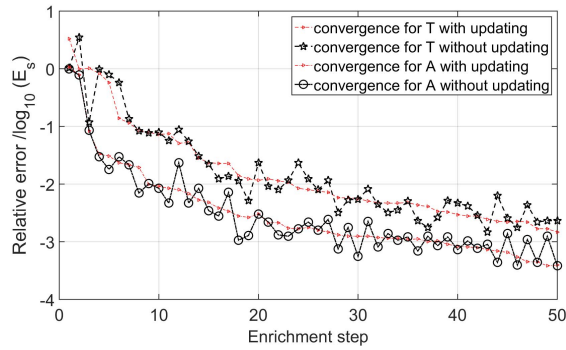


Fig. 7. Convergence rates in enrichments.

Another interesting fact of the proposed solver is that the time evaluation of A (respectively, T) over the whole domain can now be represented with 73 (respectively, 81) space-time modes (namely, space vector of size 2900×1 and time vector of size 5000×1). However, 5000 space vectors of size 2900×1 are needed with the conventional solver. For cases where all calculating results need to be stored, the PGD-based solver reduces the value size to about two orders of magnitudes lower. It can be argued that for problems where the space nodes overweight time nodes (e.g., in large-scale 3-D problems), benefits with the PGD-based non-incremental solver can be even more significant.

VI. CONCLUSION

Solving strongly coupled nonlinear magnetothermal dynamic problems using the finite element method is investigated in this paper. A PGD-based non-incremental solver is proposed. Compared with classical time integration solvers, the proposed solver is more advantageous in terms of calculating costs when a large amount of time steps is needed. In addition, accounting for nonlinearity can be incorporated in a very straightforward way. Application of the proposed solver on large-scale nonlinear multi-physics problems, incorporating parallel computing into the solver, as well as improvements to efficiency and convergence rate shall be the future extensions of this paper.

REFERENCES

- [1] L. Boucinha, A. Gravouil, and A. Ammar, "Space-time proper generalized decompositions for the resolution of transient elastodynamic models," *Comput. Methods Appl. Mech. Eng.*, vol. 255, pp. 67–88, Mar. 2013.
- [2] F. Chinesta, A. Ammar, and E. Cueto, "Recent advances and new challenges in the use of the proper generalized decomposition for solving multidimensional models," *Arch. Comput. Methods Eng.*, vol. 17, no. 4, pp. 327–350, 2010.
- [3] A. Ammar, B. Mokdad, F. Chinesta, and R. Keunings, "A new family of solvers for some classes of multidimensional partial differential equations encountered in kinetic theory modelling of complex fluids: Part II: Transient simulation using space-time separated representations," *J. Non-Newtonian Fluid Mech.*, vol. 144, pp. 98–121, Jul. 2007.
- [4] A. Nouy, "A priori model reduction through proper generalized decomposition for solving time-dependent partial differential equations," *Comput. Methods Appl. Mech. Eng.*, vol. 199, pp. 1603–1626, Apr. 2010.
- [5] A. Ammar, M. Normandin, F. Daim, D. Gonzalez, E. Cueto, and F. Chinesta, "Non incremental strategies based on separated representations: Applications in computational rheology," *Commun. Math. Sci.*, vol. 8, no. 3, pp. 671–695, 2010.
- [6] M. Beringhieri, M. Gueguen, and J. C. Grandier, "Solution of strongly coupled multiphysics problems using space-time separated representations—Application to thermoviscoelasticity," *Arch. Comput. Methods Eng.*, vol. 17, no. 4, pp. 393–401, 2010.
- [7] A. Dumon, C. Allery, and A. Ammar, "Proper general decomposition (PGD) for the resolution of Navier–Stokes equations," *J. Comput. Phys.*, vol. 230, no. 4, pp. 1387–1407, 2011.
- [8] L. Boucinha, A. Ammar, A. Gravouil, and A. Nouy, "Ideal minimal residual-based proper generalized decomposition for non-symmetric multi-field models—Application to transient elastodynamics in space-time domain," *Comput. Methods Appl. Mech. Eng.*, vol. 273, pp. 56–76, May 2014.
- [9] T. Henneron and S. Clénet, "Proper generalized decomposition method applied to solve 3-D magnetoquasi-static field problems coupling with external electric circuits," *IEEE Trans. Magn.*, vol. 51, no. 6, Jun. 2015, Art. ID 7208910.
- [10] R. Pascal, P. Conraux, and J. M. Bergheau, "Coupling between finite elements and boundary elements for the numerical simulation of induction heating processes using a harmonic balance method," *IEEE Trans. Magn.*, vol. 39, no. 3, pp. 1535–1538, May 2003.
- [11] Z. Ren and A. Razek, "Computation of 3-D electromagnetic field using differential forms based elements and dual formulations," *Int. J. Numer. Model., Electron. Netw. Devices Fields*, vol. 9, pp. 81–98, Jan. 1996.
- [12] F. Bay, V. Labbe, Y. Favennec, and J. L. Chenot, "A numerical model for induction heating processes coupling electromagnetism and thermo-mechanics," *Int. J. Numer. Methods Eng.*, vol. 58, no. 6, pp. 839–867, 2003.
- [13] F. Chinesta, R. Keunings, and A. Leygue, *The Proper Generalized Decomposition for Advanced Numerical Simulations: A Primer*. New York, NY, USA: Springer-Verlag, 2003.